# Supporting Information

One-Step Synthesis of an Antimicrobial Framework based on Covalently Cross-Linked Chitosan/ Lignosulfonate (CS@LS) Nanospheres

Ravi P. Pandey, Kashif Rasool, P. Abdul Rasheed, Tricia Gomez, Mujaheed Pasha, Said A Mansour, One-Sun Lee*, Khaled A. Mahmoud*

Qatar Environment and Energy Research Institute, Hamad Bin Khalifa University

P.O. Box 34110, Doha, Qatar.
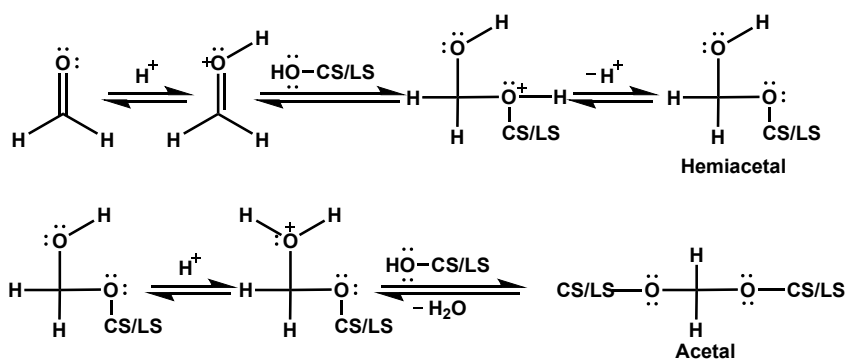
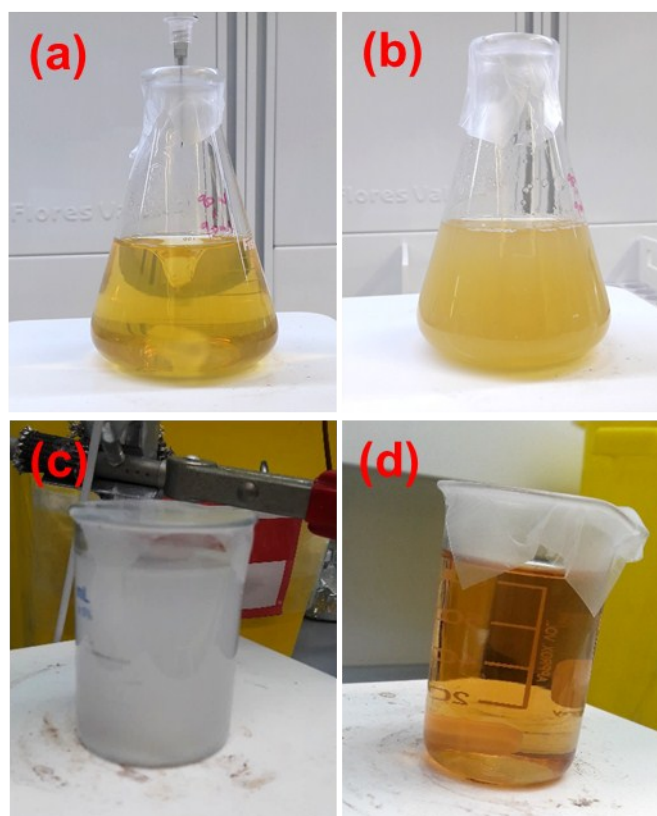**Scheme S1.** Proposed mechanism for the formation of CS@LS nanospheres.

Fig. S1. Photograph: (a) CS and LS (1:1) solution without cross-linker, (b) CS and LS (1:1) solution with cross-linker, (c) CS solution with cross-linker, and (d) LS solution with cross-linker. Each photograph taken after 2h of reaction.
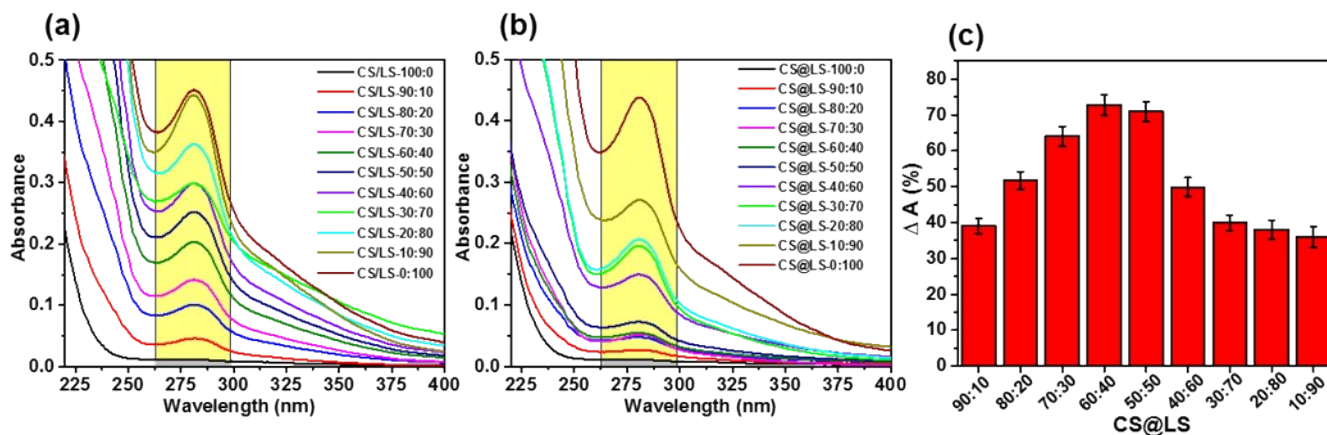
Fig. S2. (a) UV-spectra of different weight ratio (0-100%) of CS and LS mixture without cross-linking agent (kept for stirring for 2h), (b) UV-spectra of supernatant of different weight ratio of CS and LS mixture after cross-linking, obtained by centrifugation at 5000 rpm for 10 min, and (c) Percentage area under curve showing percentage of LS reacted with CS during cross-linking.
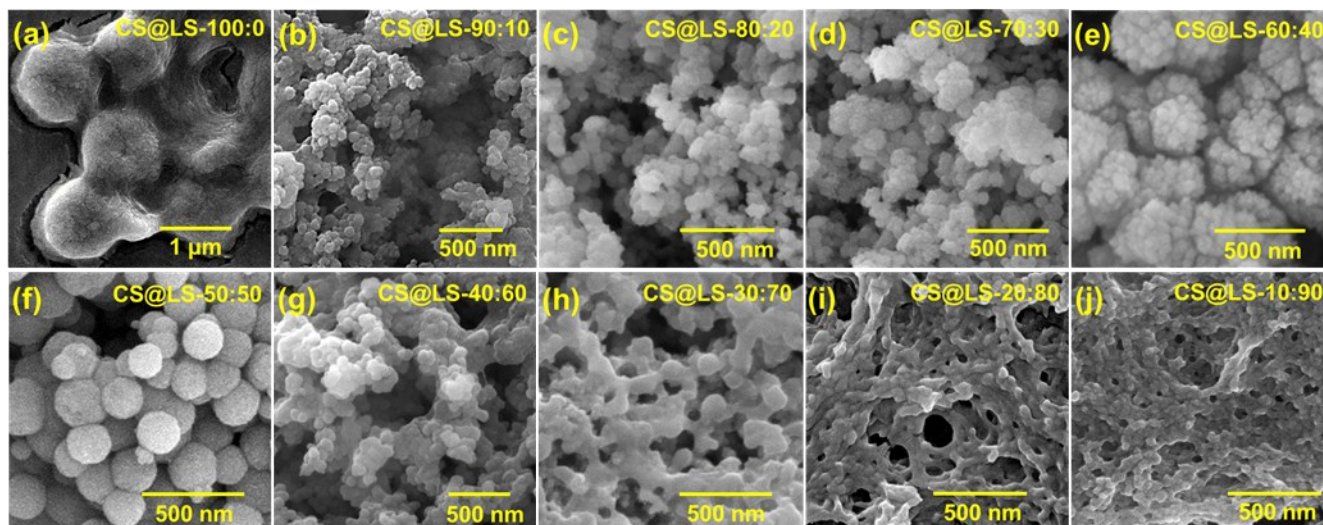

Fig. S3. SEM images for different cross-linked CS and LS composites with varying ratios of LS (0-100%).
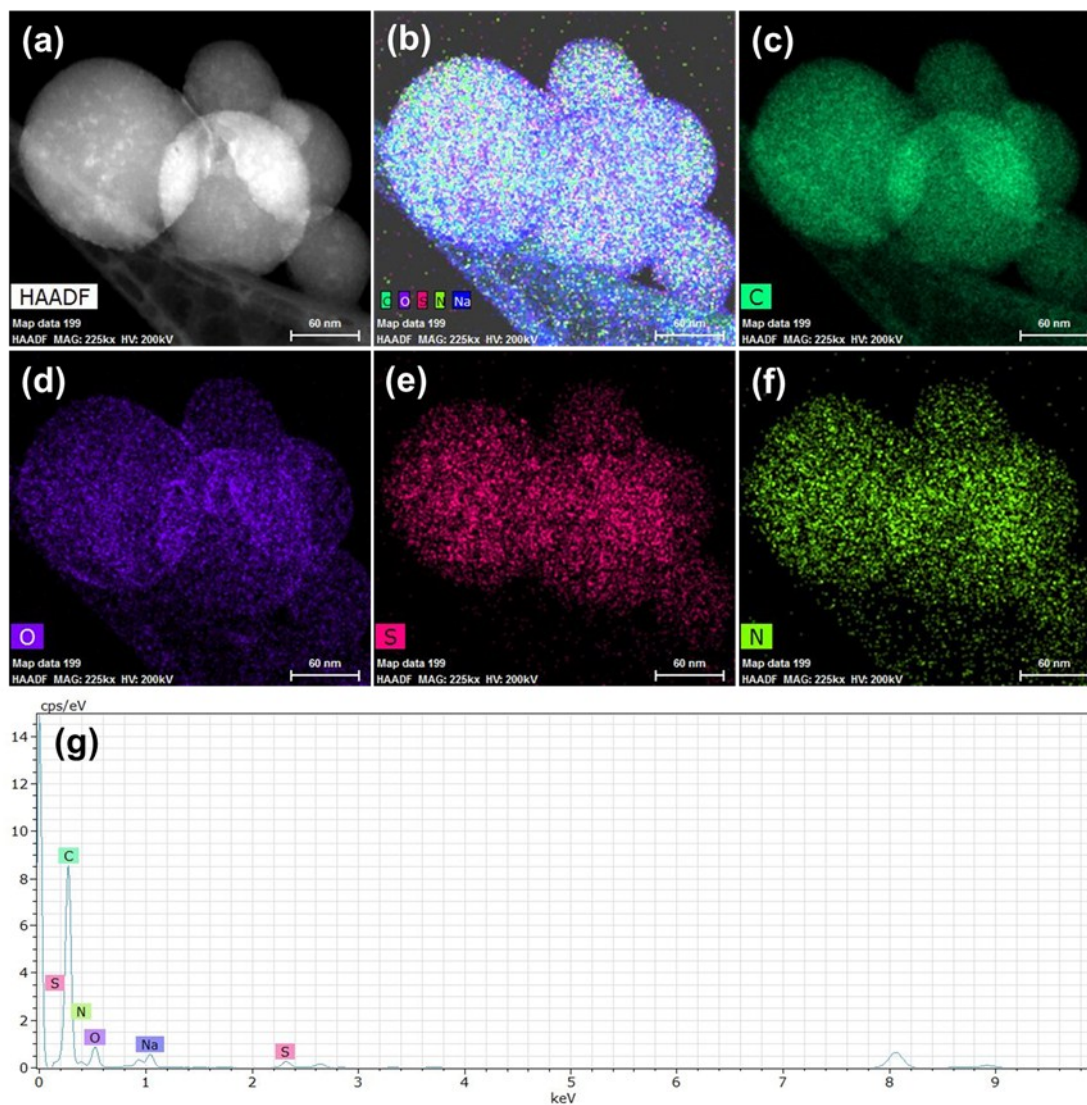
Fig. S4. (a) Scanning transmission electron microscopy (STEM) image of CS@LS-1:1 nanospheres; (b) Mix energy dispersive spectroscopy (EDS) mapping of CS@LS-1:1 nanospheres; (c-f) EDS elemental mapping of CS@LS-1:1 nanospheres with separate elements; and (g) EDS spectrum of CS@LS-1:1 nanospheres.
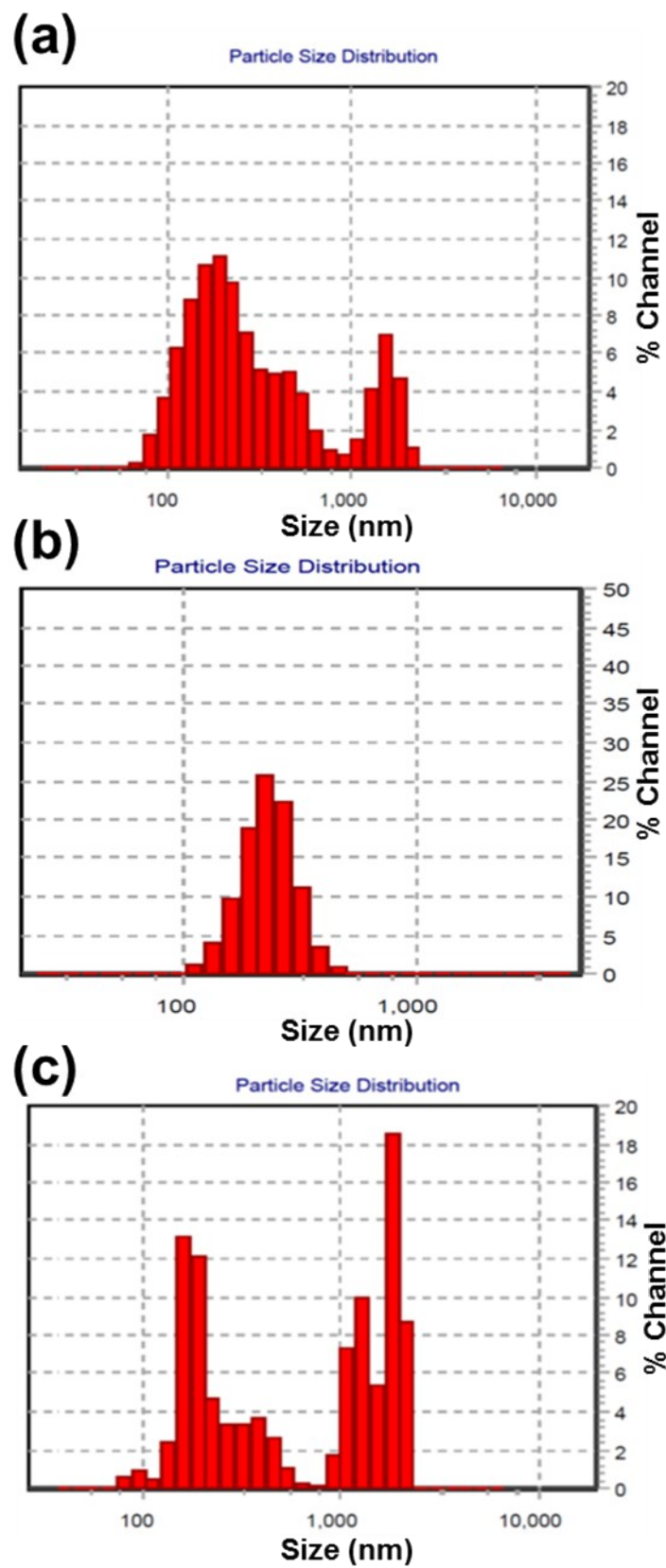
Fig. S5. Particle size measurements: (a) CS@LS-1:2, (b) CS@LS-1:1, and (c) CS@LS-2:1.

Table S1: Textural parameters of CS/LS-1:1 and CS@LS-1:1 composites.

Material	BET (m^2 g^{-1})	Pore volume (cm^3 g^{-1})	Pore diameter (nm)
CS/LS-1:1	0.9045	0.008615	31.33
CS@LS-1:1	1.3522	0.002723	11.41

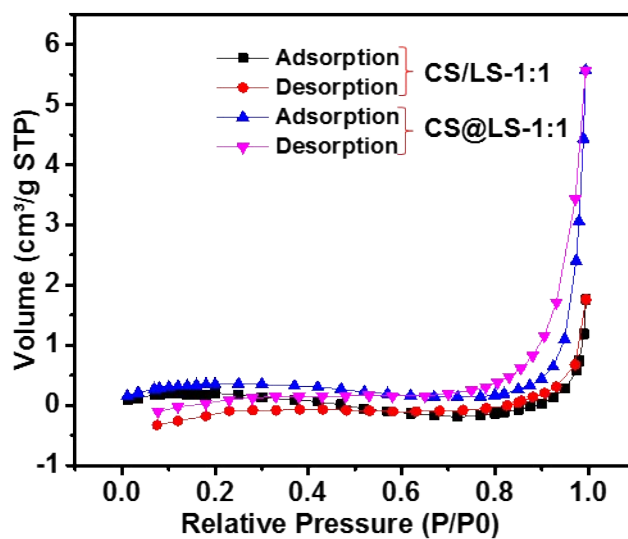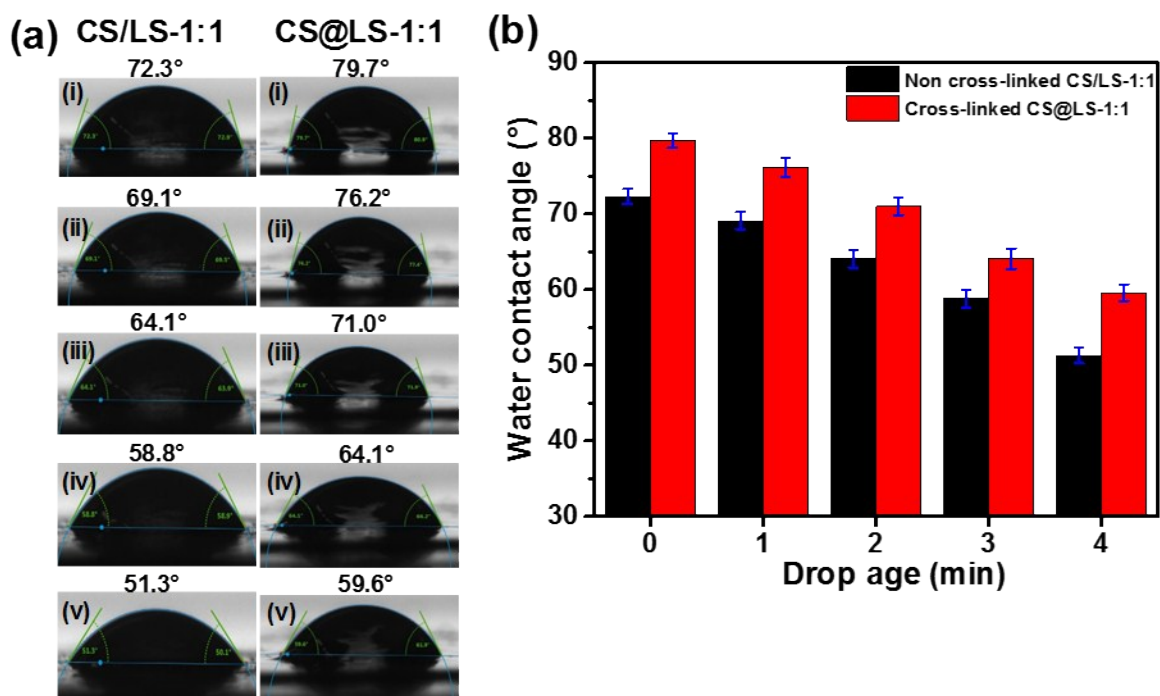**Fig. S6:** Nitrogen adsorption-desorption isotherms of CS/LS-1:1 and CS@LS-1:1 composites.

Fig S7. Water contact angle for non-cross-linked CS/LS-1:1 and cross-linked CS@LS-1:1: (a) Optical images at different time interval: (i) 0 min, (ii) 1 min, (iii) 2 min, (iv) 3 min, and (v) 4 min; and (b) Representative graph. The error bar indicates the standard deviation from the three independent measurements.
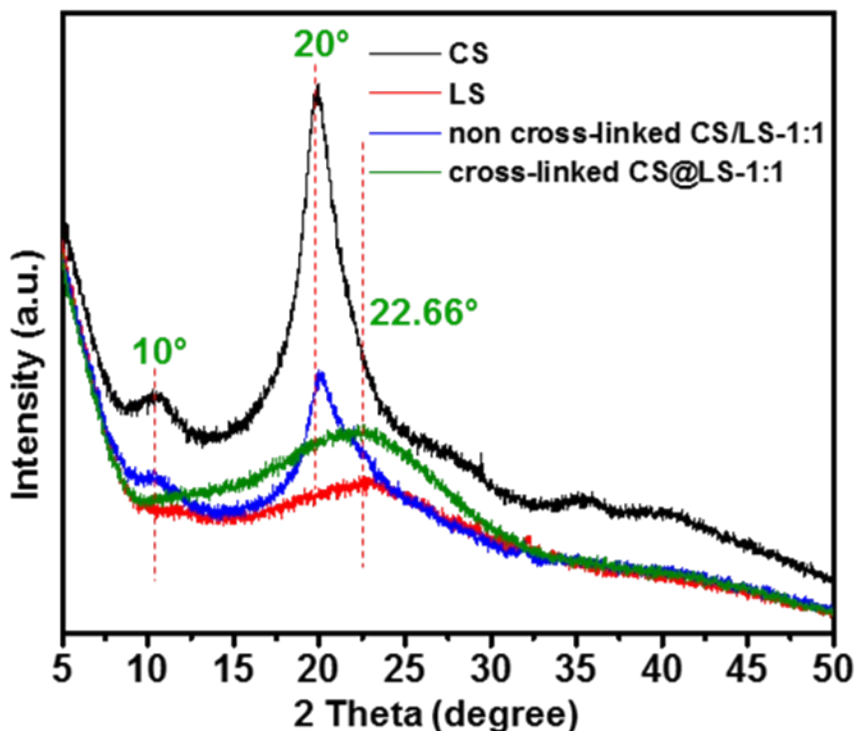
Fig S8. X-ray diffraction patterns for CS, LS, non cross-linked CS/LS-1:1 and cross-linked CS@LS-1:1.

1.   Computational Details

A coarse-grained (CG) model of chitosan and lignin is built based on the MARTINI force field (Fig. S9).[1, 2] Bond, angle, and dihedral energy functions are used for the intramolecular bonded interactions, whereas Lennard-Jones (LJ) and Coulomb functions are used for the intermolecular non-bonded interactions. The details of CG type for defining LJ parameters are shown in Table S2. The CG model of chitosan is composed of 9 protonated-glucosamine (*g*) and 6 *N*-acetylglucosamine (*n*) where we adapted a random sequence of them (*ggngnggggngngngn*) and their types and properties are based on the CG model of carbohydrates.[3, 4] For building the model of lignin, we adapted the CG model composed of three monolignol molecules where the bond between the monolignol is the ß-O-4 bond that is most abundant in nature. Even though the structure of lignin is a cross-linked polymer with high molecular masses and the degree of polymerization is difficult to measure, we adopted a simple model of lignin composed of three monolignols (Fig. S9 (c) ~ (f)) to minimize the simulation time.

We prepared two systems for comparing the self-assembly of non-cross-linked chitosan and lignin (system 1) and cross-linked chitosan and lignin (system 2). System 1 is composed of 10 molecules of chitosan, 10 molecules of lignin, 9000 water beads, 1000 ant freezing water beads, and 90 beads of chloride to electrically neutralize the system. System 2 is composed of 10 molecules of cross-linked chitosan and lignin, 9000 water beads, 1000 anti-freezing water beads,[1] and 90 beads of chloride to electrically neutralize the system.

Table S2. Name, type, and charge of CG model used for chitosan and lignin.

Molecule	Bead Name	CG Type	Charge
Chitosan	B1	P1	0
	B2	P2	0
	B3	Qd	1
	B4	P1	0
	B5	P2	0
	B6	P5	0
Lignin	BAS	P1	0
	SI1	SC5	0
	SI2	SC5	0
	SI3	SP1	0

All simulations were performed with GROMACS simulation package (version 5.0.7) with a time step of 25 fs in the NPT ensemble.[5] The pressure and temperature are maintained at 1 bar and 300 K, respectively, by means of the Berendsen method.[6] The neighbor list was updated every 10 steps using a neighbor list cutoff of r_{cut} = 1.2 nm. When interpreting the simulation results with the MARTINI model, a standard conversion factor of 4 is used to specify the speedup in CG diffusion dynamics compared to real water due to the smoothing of the potential energy landscape.[1, 7] In the remainder of this paper, we will use an effective time rather than the actual simulation time unless specifically stated. The total simulation time for each system is 8 μs, and no coordinates were constrained during the simulation.
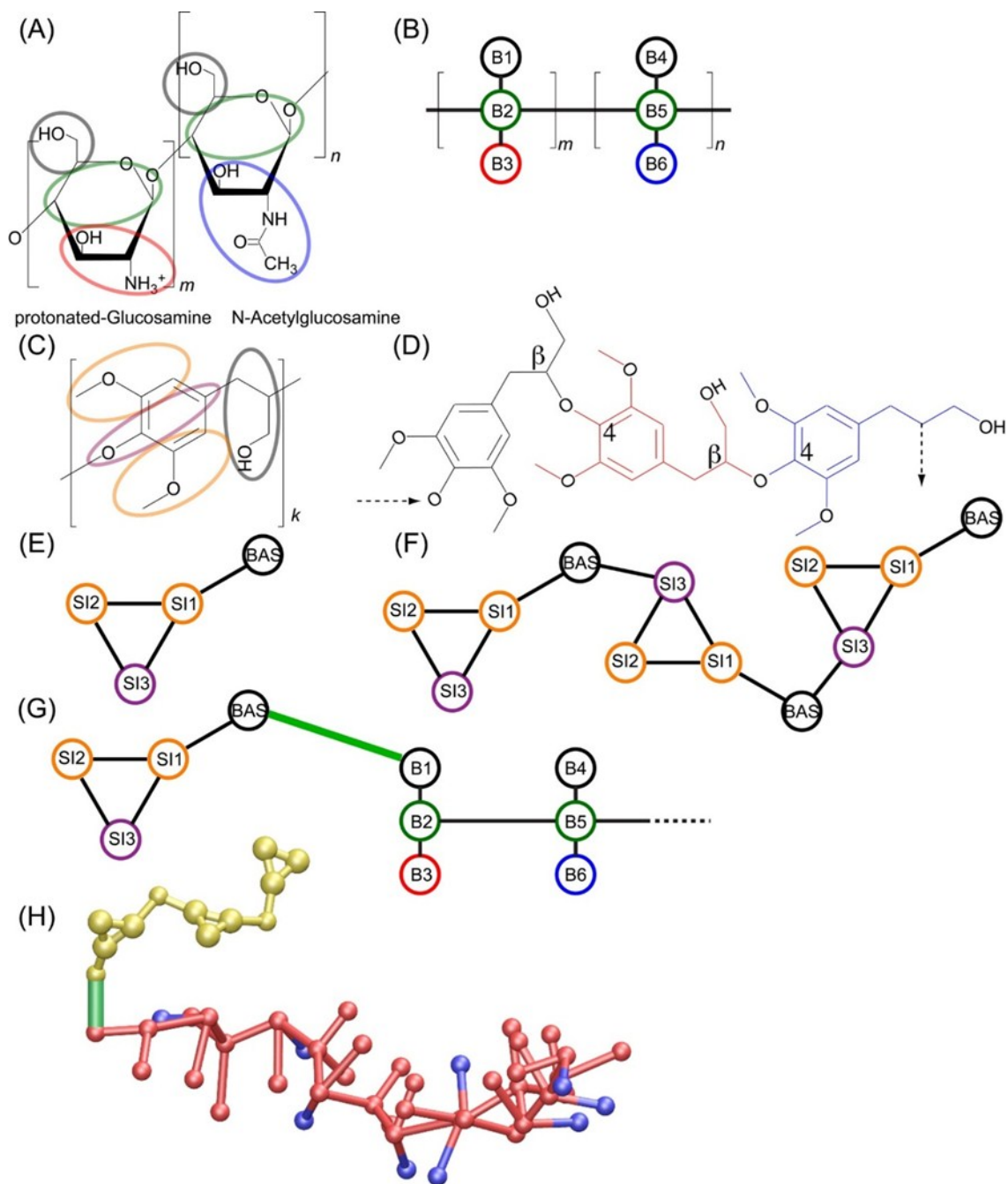
Fig. S9. (a) Schematic atomic structure of chitosan, where m = 9 and n = 6 for our simulations. The order of protonated glucosamin (g) and N-acetylglucosamine (n) is randomly chosen as ggngnggggngngngn. (b) Coarse-grained model of chitosan. (c) Schematic atomic structure of monolignol. k = 3 for our CG model of lignin. (d) Chemical structure of three monolignol connected by ß-O-4 bond which is the most abundant in nature. (e) Coarse-grained model of monolignol. (f) Coarse-grained model of three consecutively bonded monolignols. We used this structure as the CG model of lignin. (g) Schematic representation of the bond between lignin and chitosan. The bond between lignin and chitosan is represented by green line. (h) Structure of the covalently bonded lignin and chitosan used in the CG MD simulations. Lignin is

shown in yellow and the bond between chitosan and lignin is represented by the green stick model. For chitosan CG, the bead with a positive charge is shown in blue where other beads are in red.
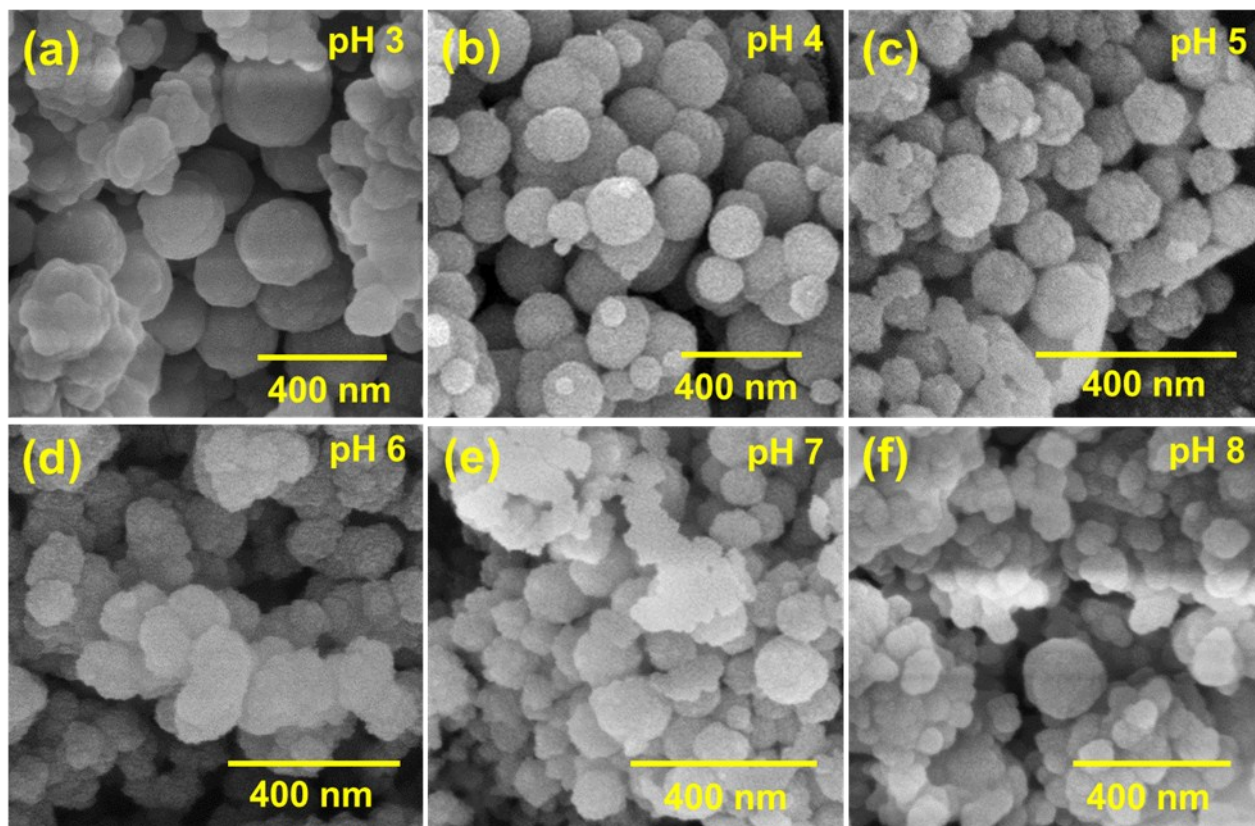

Fig. S10. SEM images of CS@LS-1:1 nanospheres kept in water at different pH for 2h (a) pH3, (b) pH4, (c) pH5, and (d) pH6, (e) pH7, and (f) pH8.

Thermal stability of CS, LS, non-cross-linked CS/LS, and cross-linked CS@LS hybrids, was analyzed by TGA (Figure S8). Weight loss up to 150 °C was observed due to the elimination of bulk and bound water from the CS@LS hybrids. Weight loss between 200 and 300 °C, was attributed to the decomposition of oxygen-containing functional groups (CO, CO_2, SO_3H, etc.).[8, 9] Beyond 300 °C, decomposition of CS and LS polymer backbone have started and finally 35, 55, 43, and 45 wt% residual mass was observed at ~499 °C, for CS, LS, non-cross-linked CS/LS-1:1, and cross-linked CS@LS-1:1 hybrids, respectively. The non-

cross-linked CS/LS-1:1 and cross-linked CS@LS-1:1 hybrids show more thermal stability than pristine chitosan might be the presence of LS moieties.
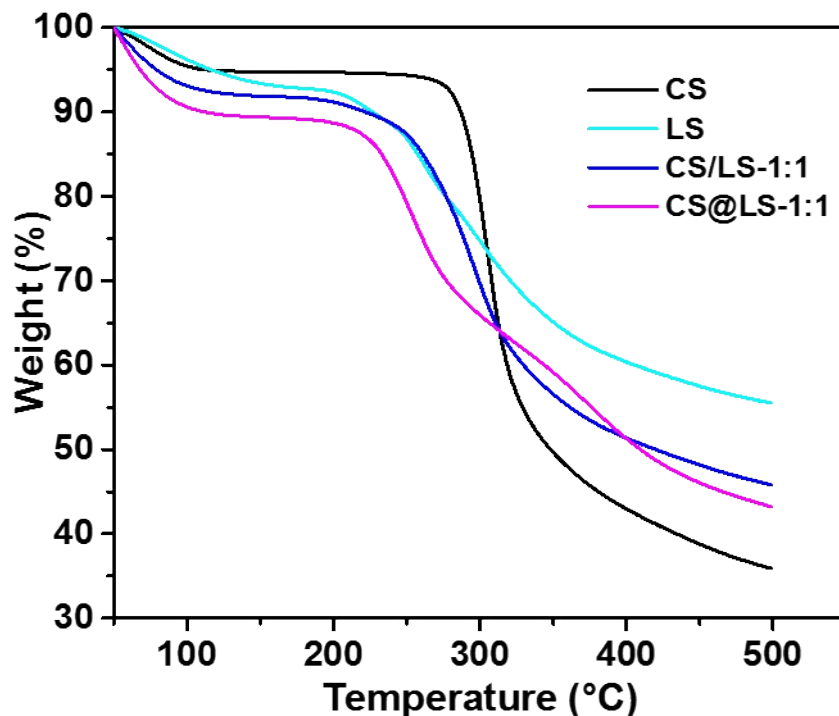

Fig. S11. TGA curves for CS, LS, non-cross-linked CS/LS-1:1 and cross-linked CS@LS-1:1.

The DSC curves of CS, LS, CS/LS-1:1, and cross-linked CS@LS-1:1 are given in Figure S9. All samples show a broad endothermic peak, around 50-150 °C, which is probably attributed to the loss of absorbed water.[10] CS showed a broad exothermic peak, around 260-310 °C centered at near 285 °C, it might be the decomposition of CS polymer backbone, which is in good agreement with the TGA analysis as given in Figure S8. The cross-linked CS@LS-1:1 showed a new endothermic peak at 220 °C, might be ascribed to reduced hydrogen bonding between CS and LS as well as the formation of covalent bond thus molecular organization due to chemical cross-linking.[11] However, non-cross-linked CS/LS-1:1 showed dominating exothermic peak, around 250-300 °C centered at near 280 °C related to CS component, which affected to the LS endothermic peak centered at 290 °C.[10]
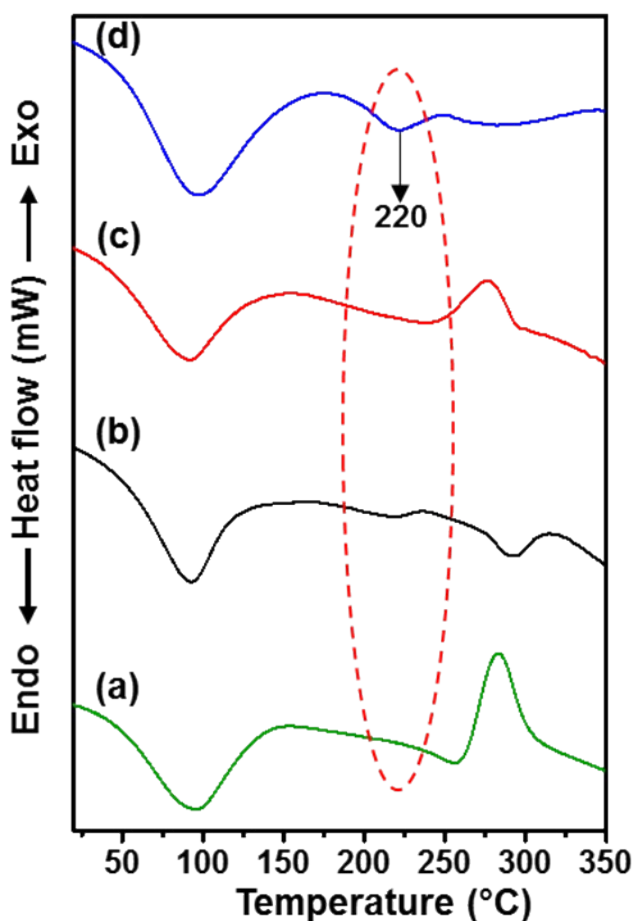
Fig. S12. Differential scanning calorimetry (DSC) curve for: (a) CS, (b) LS, (c) non-cross-linked CS/LS-1:1, and (d) cross-linked CS@LS-1:1.

Rheological properties were investigated by studying the apparent viscosities as a function of shear rate for 1 mg/mL CS, LS, cross-linked CS@LS-1:1 and non-cross-linked CS/LS-1:1 solution. At shear rate of 100 s^{-1}, the apparent viscosities were 1.479, 2.225 and 1.647 mPa.s for LS, cross-linked CS@LS-1:1 and non-cross-linked CS/LS-1:1 solutions, respectively (Figure S10 (a)). This is much lower than the CS viscosity of 4.246 mPa.s and it showed Newtonian behavior. However, the cross-linked CS@LS-1:1 and non-cross-linked CS/LS-1:1 solutions showed non-Newtonian behavior with shear-thickening following the behavior of LS.

In addition, the change of apparent viscosity of CS@LS hybrid solutions with temperature was dominated by LS behavior as shown in Figure S10 (b). When the temperature increases from 25 °C to 60

13

°C, the viscosity decreases from 0.824 to 0.558 mPa.s, 1.335 to 0.772 mPa.s, and 1.176 to 0.658 mPa.s for LS, cross-linked CS@LS-1:1 and non-cross-linked CS/LS-1:1 solutions, respectively . This was marginal variation when compared to the viscosity drop of CS solution at the same temperatures (from 4.149 to 2.059 mPa s). This intense variation is probably due to the destruction of chitosan structures and the by the polymer degradation upon heating.[12, 13] However, LS shows minor variation in the viscosity upon heating due to the cross-linking reaction occurred between the byproducts formed. The cleavage of aryl ether linkages in the lignin backbone upon heating exposed more active sites on the lignin aromatic ring that facilitates the cross-linking reaction.[14]
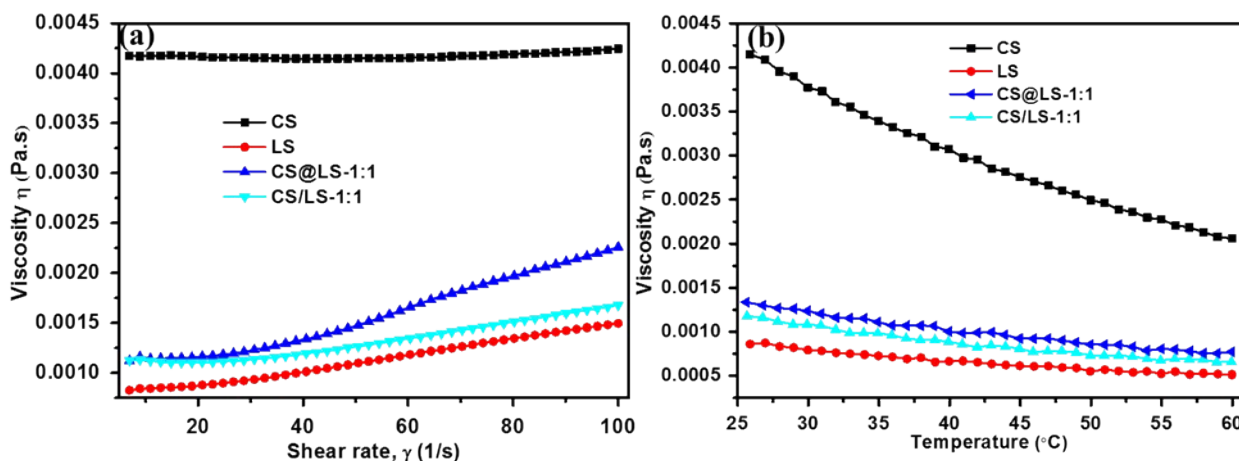

Fig. S13. (a) The plot of apparent viscosities versus shear rate and (b) the plot of apparent viscosities versus temperature.

Flow cytometry assay

A systematic analysis of the antibacterial activity of the synthesized CS@LS hybrids was performed using flow cytometry. The SYTO 9 usually labels all bacterial cells including live cells with intact membranes and dead cells with damaged membranes, whereas, propidium iodide (PI) labels only the cells with compromised membranes. So, both *E. coli* and *B. subtilis* live cells with intact membranes are labeled with fluorescent green, while cells with damaged and compromised membranes stain fluorescent red. Fluorescence analysis revealed three distinct populations comprising live, compromised and dead cells leading to a better understanding of the bactericidal mechanism of CS@LS hybrids. Both E. coli and B. Subtilis cells treated with CS@LS hybrid depicted a change of population from live to compromised and dead cells. The results showed a negligible amount of dead or lysed cells of *E. coli* and *B. subtilis* in the control samples, whereas, penetration of propidium iodide (PI) indicated the alteration and occurrence of substantial damage to the cell membrane after exposure to nanocomposites, which finally caused cell death. In the earlier assay, *E. coli* and *B. Subtilis* cells viability was studied by allowing the bacteria to grow on LB agar medium after exposure to nanocomposites. However, sometimes cells, which are with damaged membranes and scored as dead in this experiment, may be able to build up their strength and reproduce. On the other hand, certain cells with damaged membranes and declared as live in this assay may be unable to reproduce in LB medium. So the difference in cell viability measured in growth media and by flow cytometry assay may have raised form the above-mentioned facts and are in line with the earlier studies.[15]
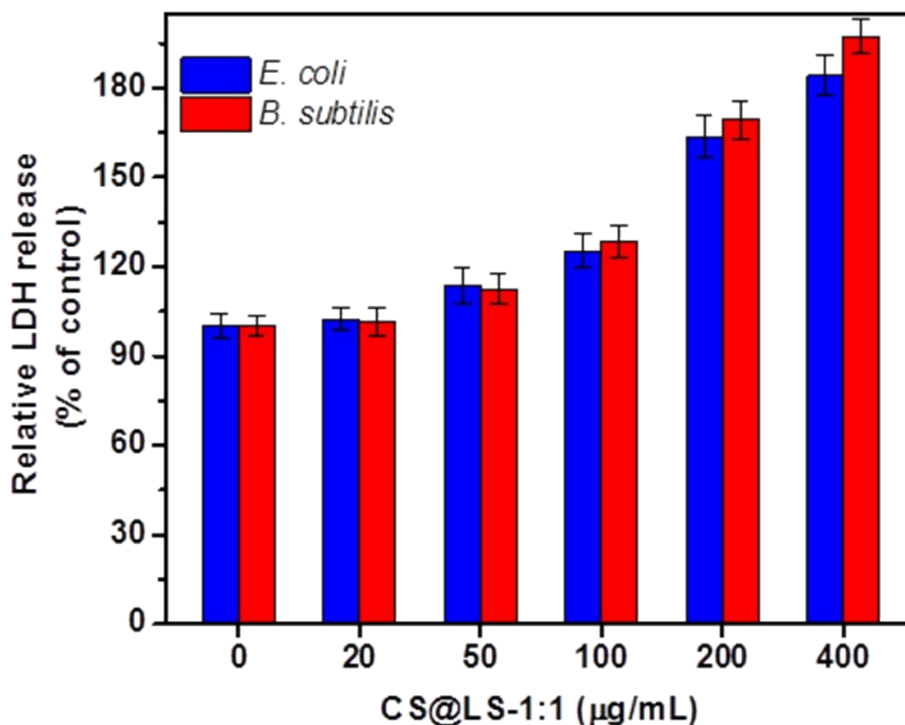
Fig. S14: LDH release from *E. coli* and *B. subtilis* cells exposed to different concentrations of CS@LS-1:1 nanospheres after 12 h of incubation time. Batch reactor without any CS@LS-1:1 nanospheres were used as control. Error bars represent the standard deviation of three independent experiments.

For the bacterial culture spiked with the synthesized CS@LS nanospheres at CS@LS-2:1, growth inhibition of E. *coli* and *B. subtilis* cells were 64.7 and 40.5% respectively and the growth inhibition of E. *coli* and *B. subtilis* cells by CS@LS-1:2, was 70.6 and 31% respectively. For the bacterial culture spiked with the synthesized CS@LS-1:1, growth inhibition of *E. coli* and *B. subtilis* cells increased to 82.4% and 61.9%, respectively, exhibiting much stronger inhibition (Figure S13). The weight ratios of CS and LS clearly affect the bactericidal activity of the synthesized nanocomposites and the most effective antimicrobial material appeared to be at CS and LS weight ratio of 1:1 and was used for the further studies as CS@LS nanospheres.
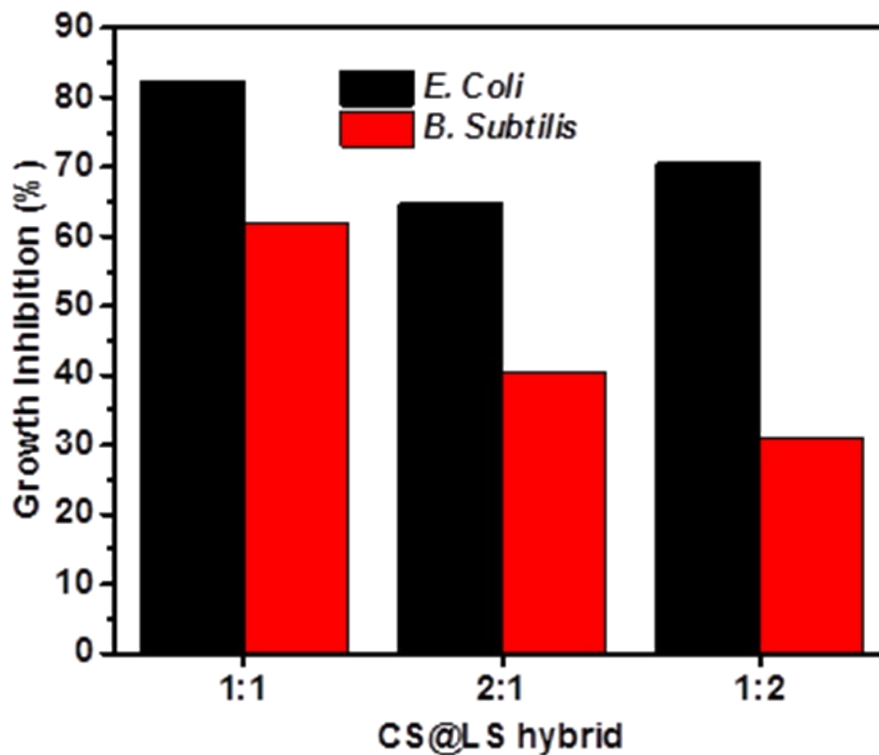
Fig. S15: *E. Coli* and *B. Subtilis* cells growth inhibition by CS@LS hybrids.

Figure S14 & S15 represents the optical images of bacterial colonies and percentage cell viability after incubating with different concentrations (0-500 μg/mL) of CS@LS-1:1. The results showed the dose-dependent bactericidal properties of CS@LS-1:1 as the number of colonies grown on the LB agar plates considerably decreased with increasing concentration of CS@LS-1:1. The percentage cell viability of both *E. coli* and *B. subtilis* was decreased and reached 0 at 500 μg/mL concentration, indicating 100% growth inhibition. Gram (-) *E. coli* appeared to be more resistant than Gram (+) *B. subtilis* at each CS@LS-1:1 concentration. The outcomes are in line with earlier studies, where higher bactericidal properties of nanoparticles were reported against Gram (+) bacteria compared to Gram (-) bacteria [16-18]. The reason for the dissimilarities in bacterial activity may be due to the difference in the cell wall structure of two bacterial strains.[19]
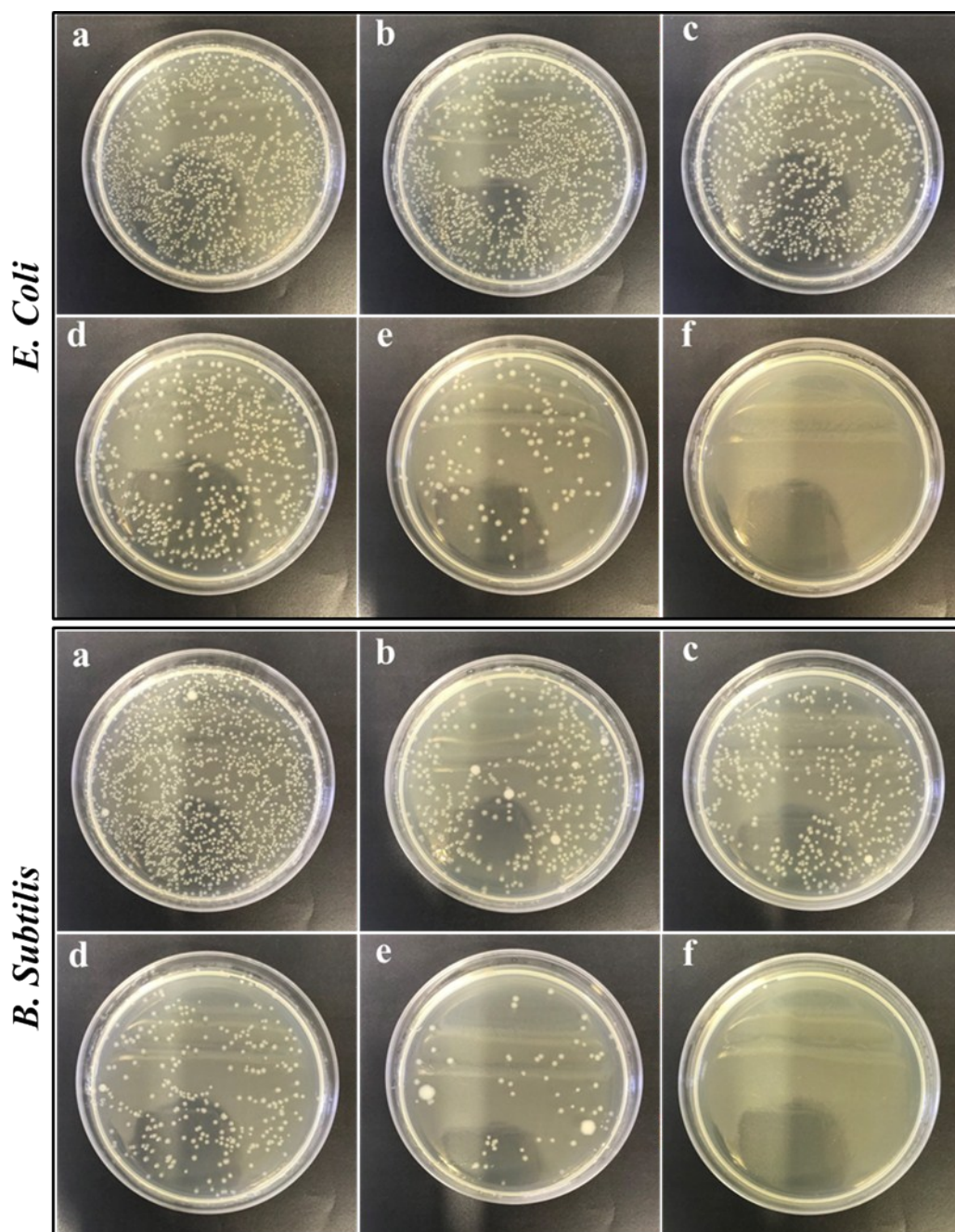
Fig. S16. Bactericidal activities of CS@LS-1:1 nanosphere in aqueous suspensions: Photographs of agar plates onto which *E. coli* (top panel) and *B. subtilis* (bottom panel) bacterial cells were recultivated after treatment for 12 h with: (a) 0 μg/mL, (b) 20 μg/mL, (c) 50 μg/mL, (d) 100 μg/mL, (e) 250 μg/mL, and (f) 500 μg/mL of CS@LS-1:1 nanosphere, respectively. Bacterial suspensions in PBS without nanospheres were used as control.
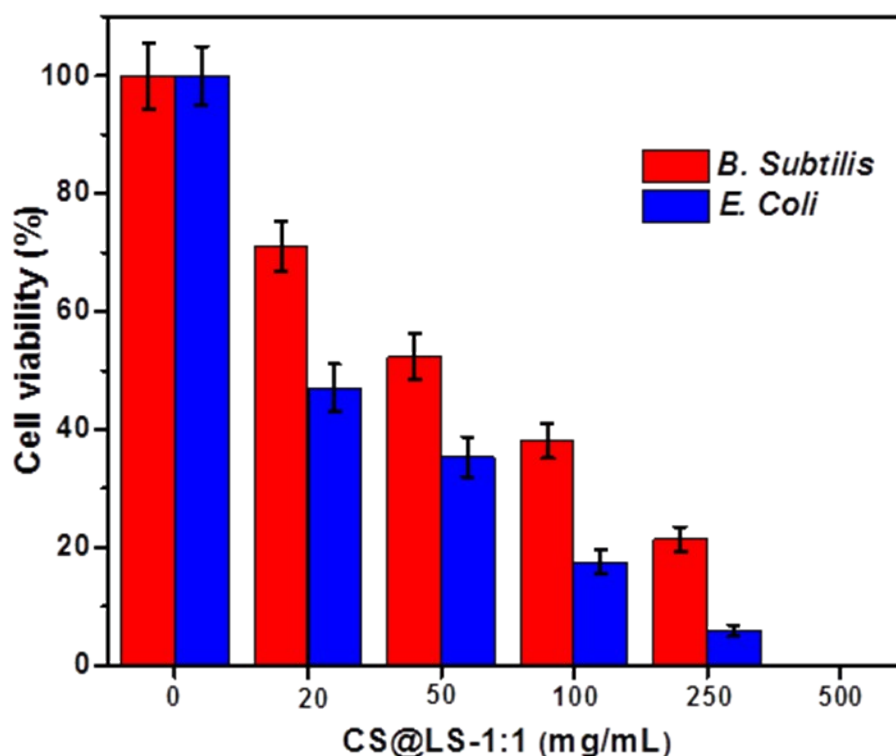
Fig. S17: Cell viability measurements of *E. coli* and *B. subtilis* treated with CS@LS-1:1 nanosphere in aqueous suspension. Bacterial suspensions (10^5 CFU/mL) were incubated with different concentrations of CS@LS-1:1 (0-500 μg/mL) at 35°C for 12 h at 150 rpm shaking speed. Survival rates were obtained by the colony forming count method. Error bars represent the standard deviation.

Minimum inhibitory concentration of synthesized CS@LS hybrids was evaluated by the turbidity method. The minimum inhibitory concentration of CS@LS nanosphere was determined by a turbidimetric method. In this method, a series of test tubes each containing 5 mL of LB broth was prepared. CS@LS nanospheres (1.5 mg/mL) were nicely dispersed in distilled water by ultra-sonication with a pH of about 6.5 and added in a test tube containing 5.0 mL of LB broth. After mixing, half the mixture was transmitted to the second tube, and similar transformations were repeated. Therefore, each test tube has a test sample solution with half of the concentration of the previous one. All the tubes were inoculated with 10 μL of

the freshly prepared bacterial suspension of *E. coli* and *B. subtilis*. The positive control was incubated with gentamicin, whereas, the blank control tubes only contained LB media. The assays were incubated at 35 °C for 24 h, the test tubes were studied for the visible signs of bacterial growth or turbidity. The lowest concentration of nanospheres that inhibited the growth of bacteria was considered as the minimum inhibitory concentration. It was found that 162.5 μg/mL is the first concentration with clarity for the aqueous LB broth for both bacterial strains. So the minimum inhibitory concentration of the CS@LS-1:1 nanospheres was found to be 162.5 μg/mL for both *E. coli* and *B. subtilis*. Furthermore, bactericidal activities of non-cross-linked CS/LS-1:1 and cross-linked CS@LS-1:1 hybrids were compared.

REFERENCES

1. S. J. Marrink, H. J. Risselada, S. Yefimov, D. P. Tieleman and A. H. de Vries, *J. Phys. Chem. B*, 2007, **111**, 7812-7824.
2. L. Monticelli, S. K. Kandasamy, X. Periole, R. G. Larson, D. P. Tieleman and S. J. Marrink, *J. Chem. Theory Comput.*, 2008, **4**, 819-834.
3. S. W. Benner and C. K. Hall, *Macromolecules*, 2016, **49**, 5281-5290.
4. C. A. Lopez, A. J. Rzepiela, A. H. de Vries, L. Dijkhuizen, P. H. Hunenberger and S. J. Marrink, *J. Chem. Theory Comput.*, 2009, **5**, 3195-3210.
5. D. Van der Spoel, E. Lindahl, B. Hess, G. Groenhof, A. E. Mark and H. J. C. Berendsen, *J. Comput. Chem.*, 2005, **26**, 1701-1718.
6. H. J. C. Berendsen, J. P. M. Postma, W. F. Vangunsteren, A. Dinola and J. R. Haak, *J. Chem. Phys.*, 1984, **81**, 3684-3690.
7. R. Baron, D. Trzesniak, A. H. de Vries, A. Elsener, S. J. Marrink and W. F. van Gunsteren, *ChemPhysChem*, 2007, **8**, 452-461.
8. R. P. Pandey, A. K. Das and V. K. Shahi, *ACS Appl. Mater. Interfaces*, 2015, **7**, 28524-28533.
9. R. P. Pandey and V. K. Shahi, *J. Power Sources*, 2015, **299**, 104-113.
10. Y. Wan, H. Wu, A. Yu and D. Wen, *Biomacromolecules*, 2006, **7**, 1362-1372.
11. A. Salam, J. J. Pawlak, R. A. Venditti and K. El-tahlawy, *Biomacromolecules*, 2010, **11**, 1453-1459.
12. O. Kuzmina, T. Heinze and D. Wawro, *ISRN Polymer Science*, 2012, **2012**, 9.
13. E. Szymańska and K. Winnicka, *Marine Drugs*, 2015, **13**, 1819-1846.
14. Y. Zhang, J.-Q. Wu, H. Li, T.-Q. Yuan, Y.-Y. Wang and R.-C. Sun, *ACS Sustain. Chem. Eng.*, 2017, **5**, 7269-7277.
15. D. B. Roszak and R. R. Colwell, *Microbiological reviews*, 1987, **51**, 365-379.
16. P. Eaton, J. C. Fernandes, E. Pereira, M. E. Pintado and F. Xavier Malcata, *Ultramicroscopy*, 2008, **108**, 1128-1134.
17. Y. Haldorai and J.-J. Shim, *Compos. Interfaces*, 2013, **20**, 365-377.
18. A. Sirelkhatim, S. Mahmud, A. Seeni, N. H. M. Kaus, L. C. Ann, S. K. M. Bakhori, H. Hasan and D. Mohamad, *Nano-Micro Lett.*, 2015, **7**, 219-242.
19. K. Rasool, M. Helal, A. Ali, C. E. Ren, Y. Gogotsi and K. A. Mahmoud, *ACS Nano*, 2016, **10**, 3674-3684.